Journal of Quantitative Spectroscopy & Radiative Transfer 217 (2018) 1–12

Contents lists available at ScienceDirect

Journal of Quantitative Spectroscopy & Radiative Transfer

journal homepage: www.elsevier.com/locate/jqsrt

Radiative properties of hedgehog-like ZnO-Au composite particles with applications to photocatalysis

B.W. Xie[a], J. Dong[b], J.M. Zhao[a], L.H. Liu[a,b,*]

[a] School of Energy Science and Engineering, Harbin Institute of Technology, Harbin 150001, China
[b] School of Energy and Power Engineering, Shandong University, Qingdao 266237, China

ARTICLE INFO

Article history:
Received 8 March 2018
Revised 29 April 2018
Accepted 29 April 2018
Available online 22 May 2018

Keywords:
Photocatalysis
Hedgehog-like composite particles
Discrete dipole approximation
Radiative properties

ABSTRACT

The recently proposed **hedgehog-like** ZnO **particles** (HPs) exhibit unusual dispersion behavior in fluids, which after being deposited with Au nanoparticles show great potential in the application of photocatalysis in both the ultraviolet and visible spectral range. Nevertheless, the radiative properties of hedgehog-like particles that largely determine the photocatalysis activity are not well understood. In this paper, models of **hedgehog-like** ZnO-**Au** composite **particles** (HP-Au) were built, and the discrete dipole approximation was applied to investigate their radiative properties in the spectral range from 0.3 to 0.8 μm. It is found that the absorption cross section of HPs increases notably with increasing number of ZnO nanorods in the spectral range from 0.3 to 0.4 μm, which can be five times that of the coated sphere for HPs having 300 nanorods. The absorption cross section of HP-Au increases with increasing amount of Au nanoparticles in the visible spectral range, but maintains at about 5 μm^2 at the resonant wavelength of Au particles for Au to Zn mass concentration ratio larger than 14%. In addition, for Au to Zn mass concentration ratio below 9%, the peak absorption cross section of the deposited Au nanoparticles is larger than that of the independent one with the largest enhancement ratio being larger than 1.5. However, the light absorption by ZnO nanorods is not enhanced by the deposited Au nanoparticles. Having the same amount of the deposited Au nanoparticles, the absorption cross section of HP-Au increases with increasing particle size. In terms of light absorption, HP-Au with a larger number of lanky ZnO nanorods that are sparsely deposited with Au nanoparticles for an Au to Zn mass concentration ratio of about 9% are preferred for the application of photocatlysis.

1. Introduction

Metal and semiconductor nanoparticles have been widely used in applications of photocatalysis, photo-thermal conversion and photoelectricity [1–4] due to their excellent optical and catalytic performance. However, nanoparticles frequently join together to form aggregate clusters in nanofluids, which significantly restricts the absorption ability of nanofluids [5–7]. Recently, Bahng et al. [8] synthesized the **hedgehog-like** ZnO **particles** (HPs), which demonstrate unusual dispersion behavior in both hydrophilic and hydrophobic media. As a wide gap semiconductor, ZnO can only absorb light in the ultraviolet (UV) range, which means that ZnO can only utilize an amount of energy that accounts for 5% of the total solar spectrum. Metal/semiconductor composite particles have been designed to realize light absorption in a broad spectral range [9] and enhance the efficiency of photocatalysis [10–13]. Using the unusual dispersion property of HPs, Wang et al. [14] synthesized the **hedgehog-like** ZnO-**Au** composite hierarchical **particles** (HP-Au) for the application of photo-thermal conversion and photocatalysis. As shown by the SEM images of the HPs in Fig. 1 [14,15], HP-Au possess spike-like surface structure and are composed of three component including the polystyrene core, the ZnO nanorods and the Au nanoparticles.

The light absorption process of photocatalyst is the precondition for the photocatalysis reaction. In the ultraviolet spectral range, the photon absorption generates the electron-hole pairs in semiconductor. The electron-hole pairs are then used for the oxidation–reduction reaction [13]. In the visible spectral range, HP-Au can act as a composite plasmonic metal/semiconductor photocatalyst, which achieve significantly stronger photocatalytic activity compared with their pure semiconductor counterparts [16–19]. The photocatalytic activity of metallized semiconductor is induced by the surface plasmon resonance of the metal nanoparticle. Specially, the role of Au nanoparticles is to create hot charge carriers through the absorption process in the mechanism of plasmon induced photocatalysis. The excited electrons with enough energy

* Corresponding author.
E-mail addresses: lhliu@hit.edu.cn, liulinhua@sdu.edu.cn (L.H. Liu).

https://doi.org/10.1016/j.jqsrt.2018.04.036
0022-4073/

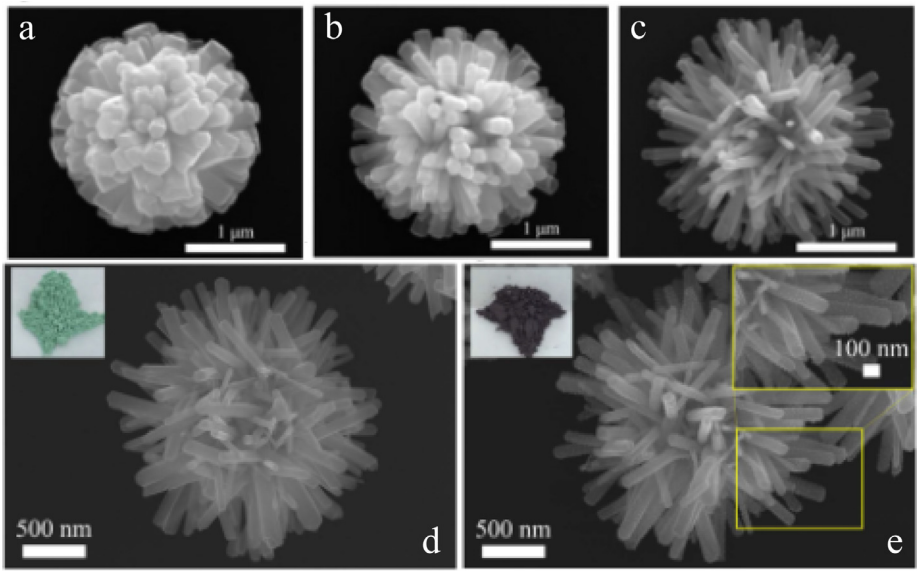

Fig. 1. SEM images of HPs and HP-Au. The shapes of HPs generated by different reaction conditions are shown in (a-c) [15]; the comparison between HPs and HP-Au can be seen in (d) and (e), the insets are the photographic images of the prepared powders [14].

overcome the barrier between the Au nanoparticles and ZnO to form electron-hole pairs [10,11]. Therefore, a larger light absorption ability of HP-Au is expected to achieve a higher photocatalysis efficiency.

It is noted that the absorption property of particles depends on the size, shape and component [20,21]. By varying the morphological features, it is found that the absorption ability of the particles can be enhanced [17,22]. Yet, the absorption property of HP-Au with respect to its morphological factors has not been well understood till now. In addition, the radiative properties of particles should be specified accurately to determine the efficiency of nanofluids and to design the solar collectors with maximum light availability [23].

Therefore, the radiative properties of HP-Au should be studied with respect to its morphological factors, as an effort to find an optimized particle morphology in terms of light absorption for the application of photocatalysis. The aim of this paper is to establish models to represent the morphological details of HP-Au and to investigate their radiative properties. The discrete dipole approximation (DDA) is applied to calculate the radiative properties of HP-Au in the spectral range from 0.3 to 0.8 μm. The effects of the particle size, the spike-like surface structure and the amount of Au nanoparticles on the radiative properties of HP-Au are analyzed. Specially, we mainly focus on the absorption ability of HP-Au that significantly impacts the photocatalysis efficiency.

2. Establishment of the model

To study the radiative properties of HP-Au, a vivid particle model should be established first to describe its main features [20], as was done by numerous researches. Liu et al. [24] developed a numerical model with hexagonal grids and barbs to represent one kind of realistic pollen particles; Dong et al. [25] built a sphere with surface spines model to represent some species of microorganisms. With such particle models, their results indicate that the spikes have a significant effect on the radiative properties of the particles. As to HP-Au, a suitable model should be established to represent the features of ZnO nanorods deposited with Au nanoparticles.

The primary structural features of hedgehog-like hierarchical particles is shown in Fig. 1. As shown, the ZnO nanorods with nearly the same size tend to grow normally to the surface of the polystyrene microsphere to finally produce HPs, thus the overall morphology of the hedgehog-like hierarchical particles is nearly spherical. The ZnO nanorods in the surface structure can be thick or lanky depending on the reaction conditions [8,14] as shown in Fig. 1(a-c). The spikes can be irregularly distributed as shown in the SEM images. However, for simplicity, we suppose that all the spikes have the same size, which are uniformly and vertically distributed on the sphere surface. The cylinders are located at uniformly distributed points on the sphere surface. As shown in Fig. 2(a), the number N of the cylinders with length l and radius r were distributed on the top of a spherical core with radius R. The cylinders and the spherical core were used to represent the ZnO nanorods and the polystyrene microsphere, respectively.

Table 1
Geometrical parameters of hedgehog-like hierarchical particles considered in this work.

Varying number N of the cylinders				Varying radius R of core			
R (μm)	N	l (μm)	r (μm)	R (μm)	N	l (μm)	r (μm)
0.50	165	0.45	0.09	0.50	300	0.75	0.05
	200	0.60	0.07	0.40		0.60	0.04
	300	0.75	0.05	0.30		0.45	0.03

By varying the N, l/R, and r/R, spike-like surface structures with various morphologies can be realized. It should be noted that the volume ratio of ZnO nanorods to the core sphere is fixed to about 3.7 in this work. The volume of ZnO nanorods can only be calculated by the number of the dipoles instead of the geometrical parameters listed in Table 1, considering that the nanorods would intersect with each other near the surface of the core sphere as shown in Fig. 1. However, the volume ratio varies within 1% among different geometrical parameters due to the volume errors in the discretization of ZnO nanorods. Different surface spike-like structures are represented by varying only the number N of ZnO nanorods in the following sections. Fig. 2(b) shows the model of HPs with different number N of ZnO nanorods. The number N of ZnO nanorods is 165, 200, 300, with l/R varied from 0.90 to 1.50 and r/R varied from 0.18 to 0.10. In addition, the radii R of the polystyrene microsphere of 0.30, 0.40 and 0.50 μm are considered while keeping N, l/R, and r/R invariable. The geometrical

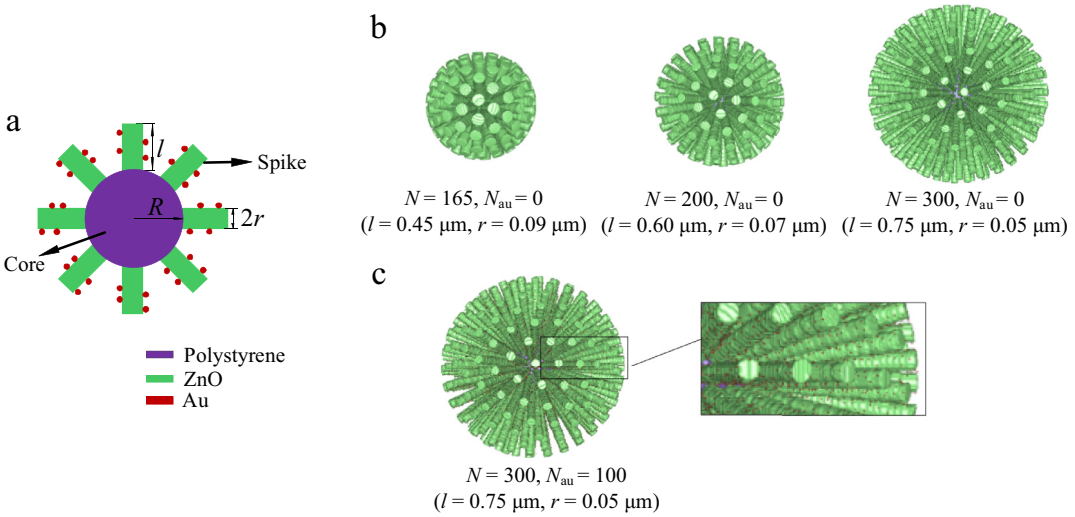

Fig. 2. The models of HPs and HP-Au: (a) geometrical parameters including the number N of cylinders, the length l of the cylinders, and the radius r of the cylindrical spike cross section; (b) HPs with different number N of cylinders, the radius R of polystyrene microsphere is 0.50 μm and the total volume of ZnO is invariable, different surface spike-like structures are represented by varying only the number N of cylinders in the following sections; (c) HP-Au with number of Au nanoparticles $N_{au} = 100$ per cylinder, the radius R_{au} of Au nanoparticles is 6.2 nm.

parameters of the hedgehog-like hierarchical particles considered in this work are illustrated in Table 1. The number N_{au} of the Au nanoparticles are varied from 100 to 300 per cylinder. Fig. 2(c) shows the model of HP-Au with 100 Au nanoparticles with radius $R_{au} = 6.2$ nm per cylinder. The Au nanoparticles are uniformly random over the side surface of the nanorods.

3. Calculation method

In this paper, we focus on the integral radiative parameters relevant for the radiative transfer simulation in nanofluids, namely, the absorption cross section C_{abs}, the scattering cross section C_{sca}, the single scattering albedo ω and the asymmetry parameter g. The radiative properties of non-spherical particles can be studied by various methods, such as the superposition T-matrix method [26,27], the discrete dipole approximation (DDA) [28,29], the finite difference time domain method [30,31], and the pseudo-spectral time domain method [32,33]. The DDA method distinguishes itself from other methods by its flexibility to deal with particles of arbitrary shape and composition. The ADDA code developed by Yurkin and Hoekstra [34] is utilized in this work. In DDA, the particle is discretized into an array of small interacting dipoles located in a regular lattice. Once the dipole moments of the cubic lattices are obtained by solving a system of linear equations, the radiative properties of the target can then be calculated [28].

The radiative properties of HPs and HP-Au were calculated in the spectral range from 0.3 to 0.8 μm. Fig. 3 illustrates the complex refractive indices m of polystyrene [35], ZnO [36] and Au [37], respectively. The refractive index of the surrounding media is supposed to be 1.33. In order to attain accurate results, the dipoles should be small enough compared with the incident wavelength, it is usually required that the parameter $|m|kd$ is smaller than 1 [38], where k is the wave number of the incident light, and d is the dipole spacing. On the other hand, the size of the dipoles should be small enough to accurately describe the structure features. In this work, the total number of dipoles ranges from about 2.4×10^6 to 2.6×10^6, and the size of the dipole is maintained to be 0.01 μm with $|m|kd$ smaller than 0.55. Nevertheless, it is difficult to further decrease the size of dipoles due to the increasing computation burden. In addition, the results were averaged over $16 \times 5 \times 8$ orientations, which is sufficient to attain orientation averaged results since the overall shape of HP-Au particle is nearly spherical.

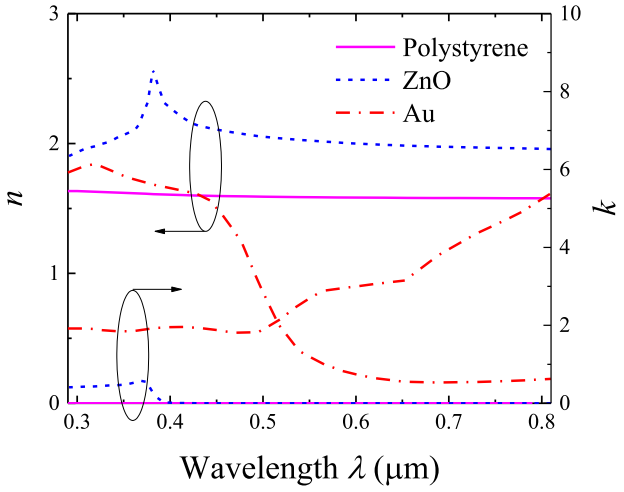

Fig. 3. The complex refractive indices m of polystyrene [35], ZnO [36] and Au [37].

Au nanoparticles should be carefully dealt with since the DDA solution tends to overestimate the absorption cross section for highly absorbing materials [39]. Nevertheless, for a small scatterer or a small amount of dipoles, many convergence problems of DDA solutions for large m are not present [34]. As shown in Fig. 1, the diameter of Au nanoparticles is about 10–15 nm which is much smaller compared with HPs with diameter of 2.5 μm. In addition, the effect of the particle shape on the radiative properties is negligible for particle sizes much smaller than the incident wavelength. Therefore, Au nanoparticle was represented by a single dipole in this work, corresponding to an equivalent volume equivalent sphere radius of 6.2 nm. Moreover, the DDA formulation should be carefully chosen. The filtered coupled dipoles (FCD) performs better than the lattice dispersion relation (LDR) for very large refractive indices [39]. However, the total amount of Au nanoparticles is much smaller than that of the polystyrene sphere and the ZnO nanorods (the volume ratio of Au to HP is less than 5%), and Au nanoparticles are sparsely distributed on the surface of HPs. Therefore, the default LDR is selected, which is expected to have good accuracy as well.

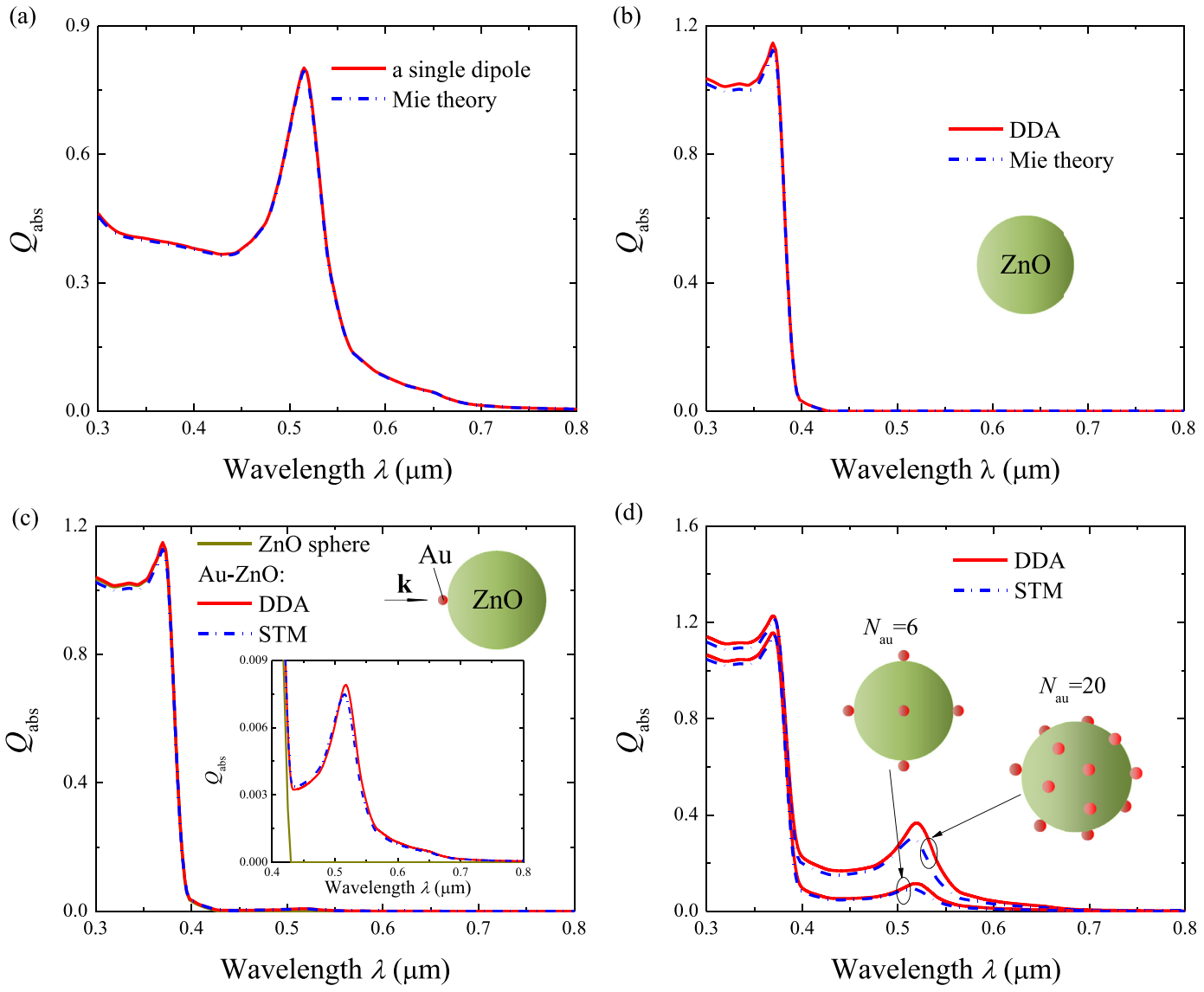

Fig. 4. (a) The absorption efficiency Q_{abs} of an Au nanoparticle calculated by a single dipole approximation and Mie theory; (b) The absorption efficiency Q_{abs} of ZnO sphere calculated by the DDA method and the Mie theory; (c-d) The absorption efficiency Q_{abs} of Au-ZnO particle calculated by the DDA method and the superposition T-matrix (STM) method [26,27]; The absorption efficiency Q_{abs} of Au-ZnO double-sphere and single ZnO sphere in the range from 0.4 to 0.8 μm is shown in the inset of (c). The radii of the Au nanoparticle and the ZnO sphere are 6.2 nm and 0.05 μm, respectively.

The accuracy of the DDA method with the Au nanoparticle approximated by a single dipole has been verified by comparing with the results of the Mie theory and the superposition T-matrix (STM) method [27]. Considering that Au nanoparticles are deposited on the surface of ZnO nanorods, the electromagnetic interaction between the Au nanoparticle and the ZnO should be well described by the DDA method. However, there are no accurate methods to calculate the radiative properties of the model composed of sphere and cylinder. Here, the cylinder is simplified to a sphere with a radius equal to 0.05 μm, which corresponds to the radius of the cylindrical spike cross section. Fig. 4 illustrates the performance of the DDA method with dipole size of 0.01 μm in estimating the absorption efficiency of (a) a single Au particle, (b) a single ZnO particle and (c-d) Au-ZnO particle. The radii of the Au nanoparticle and the ZnO sphere are 6.2 nm and 0.05 μm, respectively. The absorption efficiency of the Au-ZnO particles, as shown in the inset of Fig. 4(c-d), can be calculated accurately by the STM method [26,27].

As shown in Fig. 4(a), the absorption efficiency of single Au nanoparticle is well predicted by a single dipole with size of 0.01 μm. For a single ZnO sphere as show in Fig. 4(b), the DDA method can also well predict the absorption efficiency. In addition, as shown in Fig. 4(c), the DDA method can well predict the absorption efficiency of the Au-ZnO double-sphere particle. In the visible spectral range, the absorption of Au-ZnO particle is attributed to the Au nanoparticle. As shown in the inset of Fig. 4(c), the absorption ability of Au nanoparticle can be well described considering the effect of the ZnO sphere in the spectral range from 0.45 to 0.8 μm. For ZnO sphere deposited with more Au nanoparticles, as shown in Fig. 4(d), the absorption ability of Au-ZnO particles can also be well estimated by the DDA method. Therefore, the DDA method can well reproduce the radiative properties of HP-Au with the Au nanoparticle approximated by a single dipole.

4. Results and analysis

4.1. Radiative properties of HPs

In order to comprehensively understand the radiative properties of HP-Au and the absorption ability of the deposited Au nanoparti-

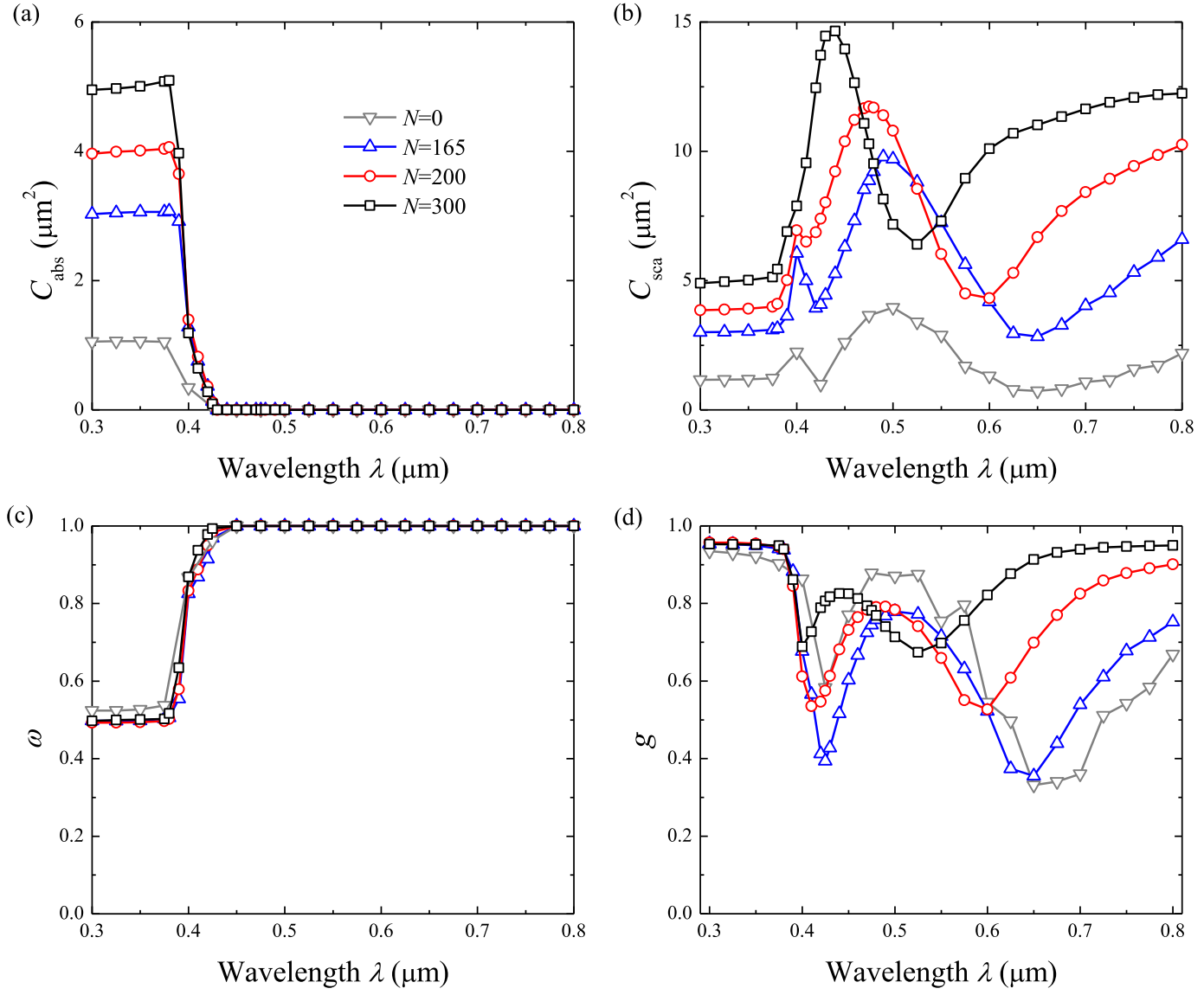

Fig. 5. The radiative properties of HPs with different number N of ZnO nanorods: (a) the absorption cross section C_{abs}; (b) the scattering cross section C_{sca}; (c) the single-scattering albedo ω; (d) the asymmetry parameter g. The radius R of the core is 0.5 μm and the total volume of ZnO is invariable. Different surface spike-like structures are represented by varying the number N of ZnO nanorods.

cles, the radiative properties of HPs should be studied first. Moreover, ZnO is a semiconductor photocatalyst with a wide spectral range gap (3.37 eV), which means that only the photon with wavelength below 368 nm can excite the electrons from the valence band to the conduction band, leaving a hole in the valence band. Therefore, the light absorption ability of HPs in the UV spectral range is of great significance in the application of photocatalysis and is analyzed in detail below.

4.1.1. Effect of surface spike-like structures

The effect of the surface spike-like structure on the radiative properties of HPs is investigated. It is noted that different surface spike-like structures are only represented by the number N of ZnO nanorods while keeping the total volume of ZnO invariable. Fig. 5 shows the integral scattering properties of HPs with different number N of ZnO nanorods, the radius R of core is 0.5 μm and the total volume of the ZnO is fixed. For comparison, the results of the polystyrene-ZnO coated sphere ($N=0$) are also depicted in Fig. 5. As shown in Fig. 5(a), the absorption cross section of HPs changes very little in the spectral range from 0.3 to 0.38 μm but decreases sharply in the spectral range from 0.38 to 0.42 μm. HPs have no absorption in the visible spectral range. In addition, the absorption cross section of HPs increases obviously with increasing number of ZnO nanorods in the spectral range from 0.3 to 0.4 μm. For HPs with 300 ZnO nanorods, the absorption cross section is about 5 μm^2 which is five times that of the polystyrene-ZnO coated sphere ($N=0$). These phenomena can also be found in Ref. [25] and are explained below. With increasing number of ZnO nanorods, the surface area of HPs increases and the multi-scattering intensity between the ZnO nanorods becomes stronger, therefore, the light absorption ability increases. Since photocatalysis is a surface reaction, HPs with lankier ZnO nanorods have larger effectiveness of photocatalysis in terms of light absorption.

As shown in Fig. 5(b), the scattering cross section changes very little in the spectral range from 0.3 to 0.38 μm, shows a sharp peak in the spectral range from 0.4 to 0.6 μm and then increases monotonously with wavelength in the spectral range from 0.6 to 0.8 μm. With decreasing number of ZnO nanorods, the scattering cross section decreases obviously and its peak position tends to red shift, due to the decreased overall dimension of the HPs. As

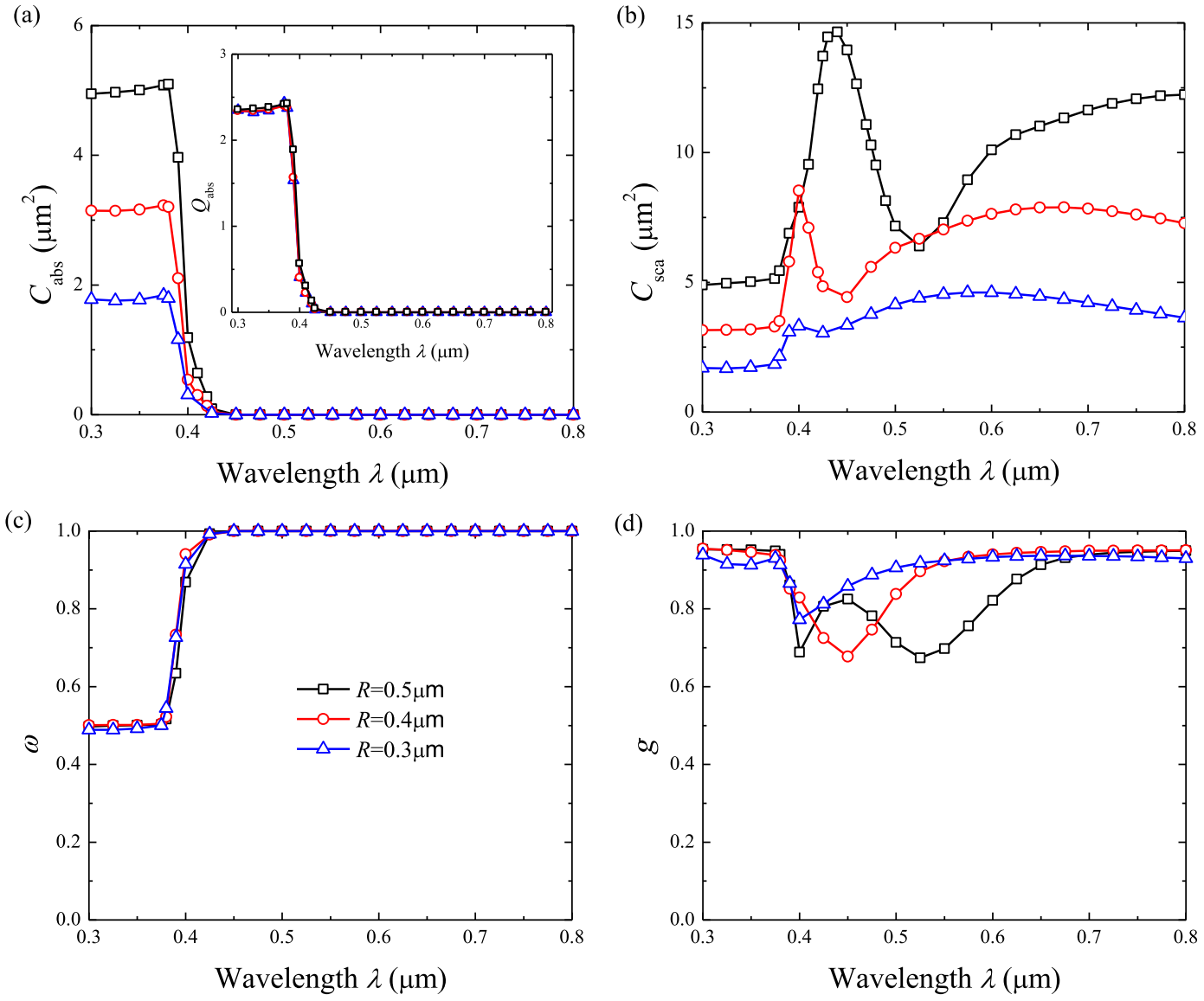

Fig. 6. The radiative properties of HPs with different particle size: (a) the absorption cross section C_{abs}; (b) the scattering cross section C_{sca}; (c) the single-scattering albedo ω; (d) the asymmetry parameter g. The inset of (a) is the absorption efficiency Q_{abs} of HPs with different particle size. The number N of ZnO nanorods is 300 and the size of HPs is represented by the radius R of the core with the same morphology parameters N, l/R, and r/R of surface spike-like structures.

shown in Fig. 5(c), the single scattering albedo is insensitive to the number of ZnO nanorods in the spectral range from 0.3 to 0.8 μm. In addition, the single scattering albedo is almost constant with a value of about 0.5 in the spectral range from 0.3 to 0.4 μm. The asymmetry parameter is independent of the number of ZnO nanorods and the wavelength in the spectral range from 0.3 to 0.38 μm with a value of about 0.95 as shown in Fig. 5(d), while in the visible spectral range it is sensitive to the wavelength and tends to increase with increasing number of ZnO nanorods in the visible spectral range.

4.1.2. Effect of particle size

The effect of particle size of HPs on the radiative properties is studied. In this work, the size of HPs is represented by the radius R of the core with the same morphology parameters, i.e. the same N, l/R, and r/R of surface spike-like structures. Fig. 6 illustrates the integral scattering properties of HPs with different particle size while the number N of cylinders is fixed at 300. As shown in Fig. 6, the absorption cross section of HPs increases significantly with increasing particle size, whereas the absorption efficiency is almost independent of the particle size as shown in the inset of Fig. 6(a). Therefore, the absorption ability of HPs largely depends on the morphology of surface structure but is almost independent of particle size.

As can be seen in Fig. 6(b), the scattering cross section of HPs decreases with decreasing size of HPs in the spectral range from 0.3 to 0.8 μm, and its peak position tends to blue shift. In addition, for particle with smaller size, the spectral distribution of the scattering cross section is flat, while for particle with larger size a prominent peak of the scattering cross section can be observed. The single-scattering albedo is almost independent of the particle size as shown in Fig. 6(c). The asymmetry parameter is insensitive to the particle size in the spectral range from 0.3 to 0.4 μm and from 0.65 to 0.8 μm, while in the spectral range from 0.4 to 0.65 μm it tends to increase with decreasing particle size. Overall, with the same surface structure parameters, the effect of particle size is only obvious on the scattering cross section.

4.2. The radiative properties of HP-Au

The photocatalysis activity of HP-Au can be induced by the UV light as well as the visible light [11]. In the UV spectral range,

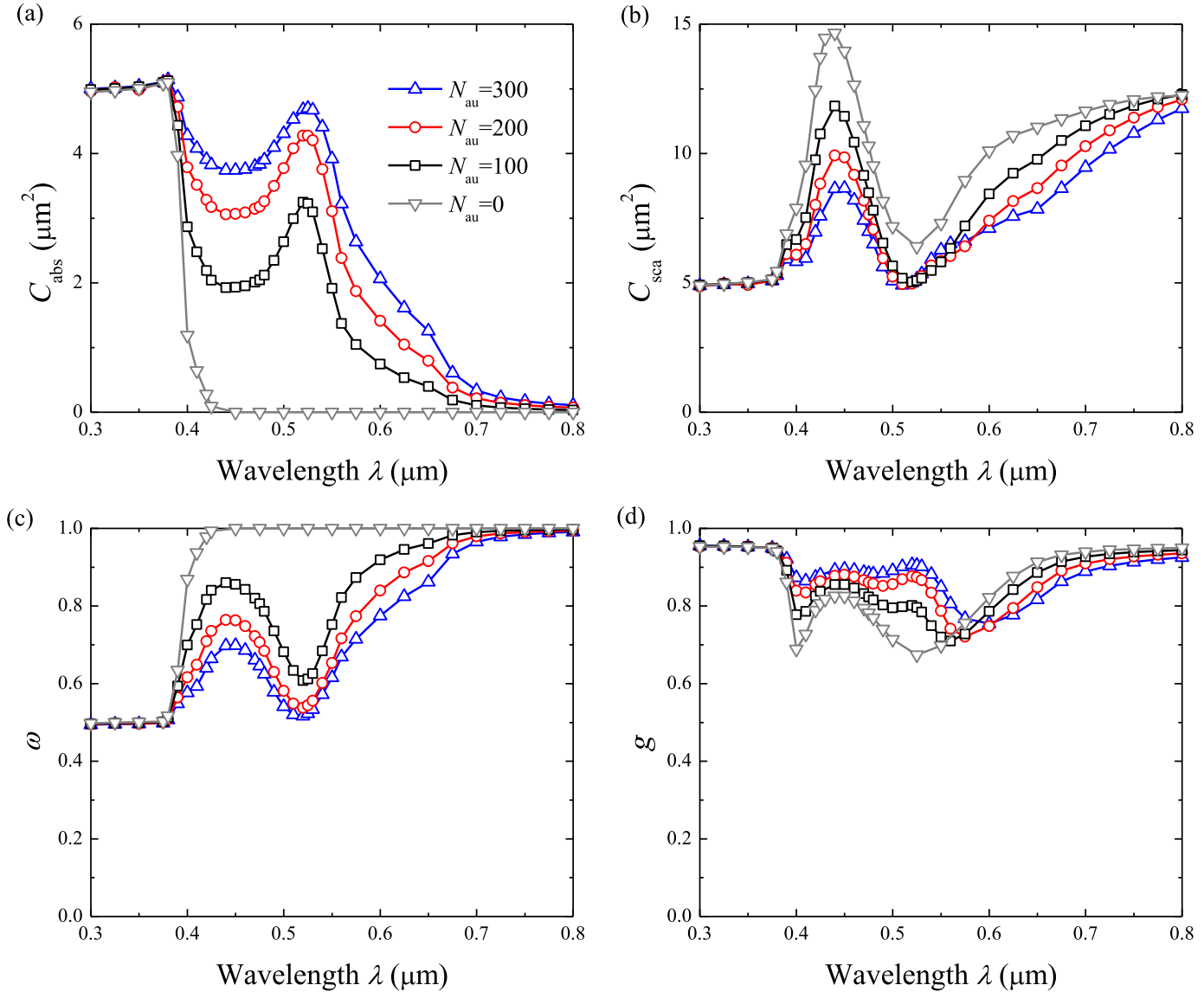

Fig. 7. The radiative properties of HP-Au particle with different number N_{au} of Au nanoparticles: (a) the absorption cross section C_{abs}; (b) the scattering cross section C_{sca}; (c) the single-scattering albedo ω; (d) the asymmetry parameter g. The radius R of the core is 0.5 μm and the number N of ZnO nanorods is 300.

the light absorption of ZnO generates the electron-hole pairs that lead to the photocatalysis as discuss above. The schottky barrier forming at the interface between Au nanoparticles and ZnO effectively separates the excited electron and hole, thus the photocatalytic activity of metallized semiconductor increases [40,41]. In the visible spectral range, HP-Au can act as a composite plasmonic metal/semiconductor photocatalyst. In the mechanism of plasmon induced photocatalysis, the localized surface plasmon resonances of Au nanoparticles generates highly excited electron-hole pairs for photocatalysis [11]. Overall, for HP-Au, the useful spectral range and the source of free electrons are different under the two photocatalysis mechanisms.

4.2.1. Effect of the number of deposited Au nanoparticles

The effect of the amount of Au nanoparticles on the radiative properties of HP-Au is investigated. Fig. 7 demonstrates the integral scattering properties of HP-Au with different number N_{au} of Au nanoparticles. HPs with lanky ZnO nanorods exhibit stronger light absorption ability and better dispersion performance than those with thick ZnO nanorods [8]. In addition, the absorption properties of HPs are almost independent of the particle size as discussed above. Therefore, only the radiative properties of HP-Au with the number of ZnO nanorods $N = 300$ and the radius of the core $R = 0.5$ μm are investigated. As shown in Fig. 7, the effect of the number of Au nanoparticles on the four integral scattering properties of HP-Au is strong in the visible spectral range but weak in the spectral range from 0.3 to 0.4 μm. Specially, the absorption cross section and the single scattering albedo increase obviously, but the scattering cross section decreases in the visible spectral range with increasing number of Au nanoparticles. In addition, the asymmetry parameter increases with increasing number of Au nanoparticles in the spectral range from 0.4 to 0.6 μm, while it decreases in the spectral range from 0.6 to 0.8 μm.

It should be noted that the absorption cross section of HP-Au is almost unchanged with increasing amount of Au nanoparticles in the spectral range from 0.3 to 0.4 μm. Considering that Au nanoparticles are widely distributed on the surface of ZnO nanorods, the interaction between Au nanoparticles and ZnO nanorods can be described by the double sphere model as shown in the inset of Fig. 4(c). Fig. 8 shows the normalized electric field intensity $|E/E_0|^2$ of Au-ZnO double sphere particle at the wavelengths of 0.35 μm and 0.52 μm, respectively. As can be seen in Fig. 8, the deposition

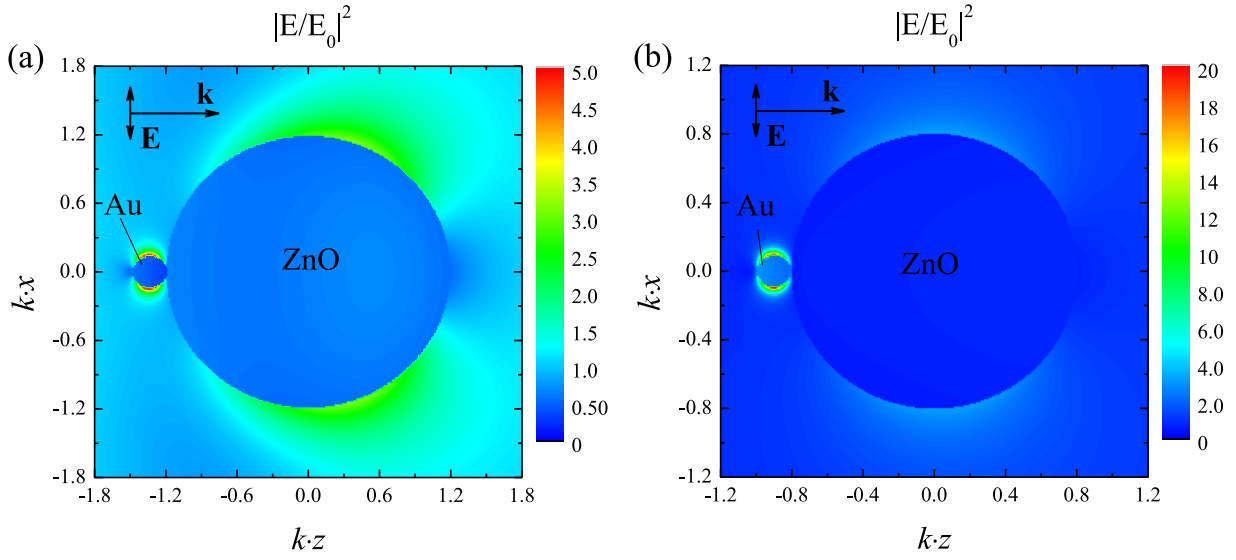

Fig. 8. The normalized electric field intensity $|E/E_0|^2$ of Au-ZnO double sphere particle at the wavelength of (a) 0.35 μm and (b) 0.52 μm. E_0 is the incident electric field intensity. The radii of the Au nanoparticle and the ZnO sphere are 6.2 nm and 0.05 μm, respectively. The normalized electric field intensity is calculated by the superposition T-matrix method (STM) [26].

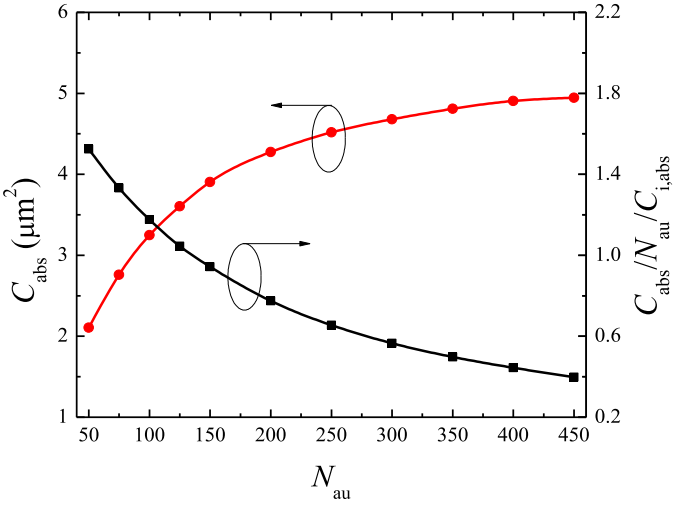

Fig. 9. The absorption cross section C_{abs} of HP-Au at the wavelength of 0.52 μm and its ratios ($C_{abs}/N_{au}/C_{i,abs}$) to that of independent Au nanoparticle as a function of the number N_{au} of Au nanoparticles per ZnO nanorod. $C_{i,abs}$ is the absorption cross section of a single Au nanoparticle, which is calculated by the Mie theory [21].

of Au nanoparticles do not lead to the increase of light absorption of the ZnO sphere. The absorption cross section of HP-Au peaks at the wavelength of 0.52 μm, due to the localized surface plasmon resonances of Au nanoparticles as shown in Fig. 8(b). Thus, the light absorption of HP-Au in the visible spectral range is only attributed to Au nanoparticles.

The localized surface plasmon resonance of Au nanoparticles plays a significant role in determining the photocatalysis activity of HP-Au. Fig. 9 shows the absorption cross section C_{abs} of HP-Au and its ratio ($C_{abs}/N_{au}/C_{i,abs}$) to that of a single Au nanoparticle as a function of the number of Au nanoparticles per ZnO nanorod at the wavelength of 0.52 μm. The absorption cross section $C_{i,abs}$ of the Au nanoparticle is calculated by the Mie theory [21]. Actually, the absorption of HP-Au is caused by the absorption of the deposited Au nanoparticles since ZnO has no absorption in the visible spectral range (the imaginary part of the complex refractive index of ZnO is zero as shown in Fig. 3). As shown in Fig. 9, the absorption cross section of HP-Au increases with increasing amount of Au nanoparticles, and the increase of the absorption cross section is sharp when the number of Au nanoparticles is less than 125 (the Au to Zn mass concentration ratio is about 9%). However, when the number of Au nanoparticles is larger than 200 (the Au to Zn mass concentration ratio is about 14%), further deposition of Au nanoparticles will not obviously increase the absorption cross section of HP-Au, since the shielding effect is significant for dense particle system, which is in line with the analysis by Okada et al. [6]. Moreover, the ratio $C_{abs}/N_{au}/C_{i,abs}$ decreases with increasing amount of Au nanoparticles. The ratio $C_{abs}/N_{au}/C_{i,abs}$ is larger than unity when the number of Au nanoparticles is less than 125 (the Au to Zn mass concentration ratio is about 9%), and can exceed 1.5 with 50 Au nanoparticles deposited (the Au to Zn mass concentration ratio is about 4%). This phenomenon can be explained as below. For HP-Au deposited with a small amount of Au nanoparticle, the shielding effect is weak. Therefore, the multi-scattering intensity in the spike-like surface structure is strong enough to enhance the absorption of Au nanoparticles.

4.2.2. Effect of particle size

Fig. 10 demonstrates the integral scattering properties of HP-Au with different particle sizes, the number N_{au} of the Au nanoparticles is 100 and the number N of ZnO nanorods is 300. The size of HPs is represented by the radius R of the core. As shown in Fig. 10(a), the absorption cross section of HP-Au with the same amount of Au nanoparticles increases with increasing particle size in the spectral range from 0.3 to 0.6 μm. Since the effect of the Au nanoparticles on the absorption is weak in the spectral range from 0.3 to 0.42 μm, the increase in the absorption of HP-Au is mainly caused by the increasing volume of the ZnO nanorods. In the spectral range from 0.42 to 0.6 μm, however, the increase of absorption cross section of HP-Au is attributed to the Au nanoparticles since ZnO has no absorption in visible spectral range. This phenomenon can be explained as below. For smaller size of HP-Au, which means that Au nanoparticles are distributed in a smaller space, the shielding effect leads to the decrease of light absorption. Nevertheless, the absorption cross section of HP-Au is independent of the size of HP-Au in the spectral range from 0.6 to 0.8 μm, due to the fact that the shielding effect is weak for particles with less absorption

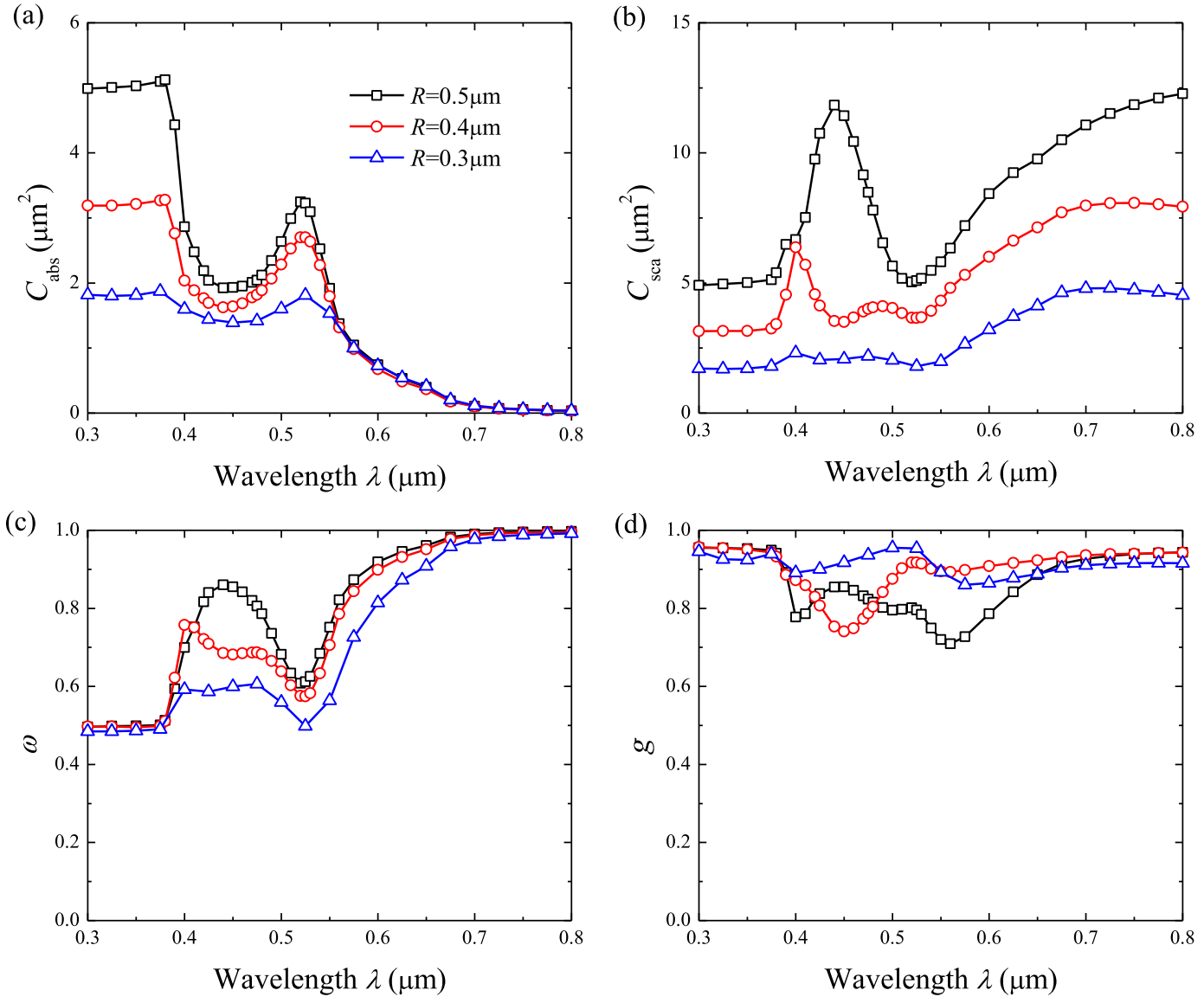

Fig. 10. The radiative properties of HP-Au particle with different radius R of the core: (a) the absorption cross section C_{abs}; (b) the scattering cross section C_{sca}; (c) the single-scattering albedo ω; (d) the asymmetry parameter g. The number N_{au} of Au nanoparticles is 100 and the number N of cylinders is 300.

[6]. The spectral position of absorption peak is unchanged with increasing size of HP-Au.

Moreover, as can be seen in Fig. 10(b) and (d), the effect of particle size on the scattering cross section and the asymmetry parameter of HP-Au is similar to that of the HPs as discussed above. For HP-Au with core radius of 0.3 μm, the asymmetry parameter deviates very little from unity in the spectral range from 0.3 to 0.8 μm, which indicates that the scattering intensity is mostly distributed in the forward direction. The single-scattering albedo increases with increasing size of HP-Au in the visible spectral range as show in Fig. 10(c), whereas in the spectral range from 0.3 to 0.4 μm the dependence of the single scattering-albedo on particle size is weaker.

4.3. Simplified equivalent models

In practical applications, simplified equivalent models are frequently applied to calculate the radiative properties of real particles due to their unparalleled simplicity. Dong et al. [25] investigated the performances of the equivalent volume sphere (EVS) and the core-shell sphere (CSS) models in estimating the radiative properties of homogeneous particle with surface spine-like structure, their result indicated that the CSS model is better than the EVS model. In this work, the EVS and the CSS model are considered, as shown in Fig. 11. The radius R_{EVS} of the EVS model can be calculated by:

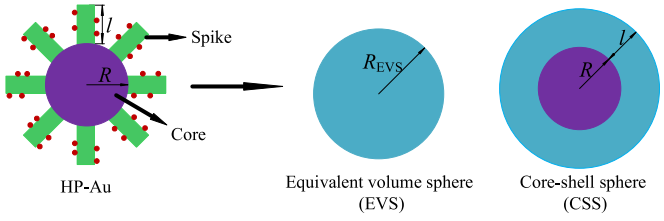

Fig. 11. The equivalent volume sphere (EVS) and the core-shell sphere (CSS) models for HP-Au. The inner core of the CSS model is the polystyrene sphere, and the outer shell represents the spike zone.

$$R_{EVS}=\sqrt[3]{V_1+V_2+V_3} \quad (1)$$

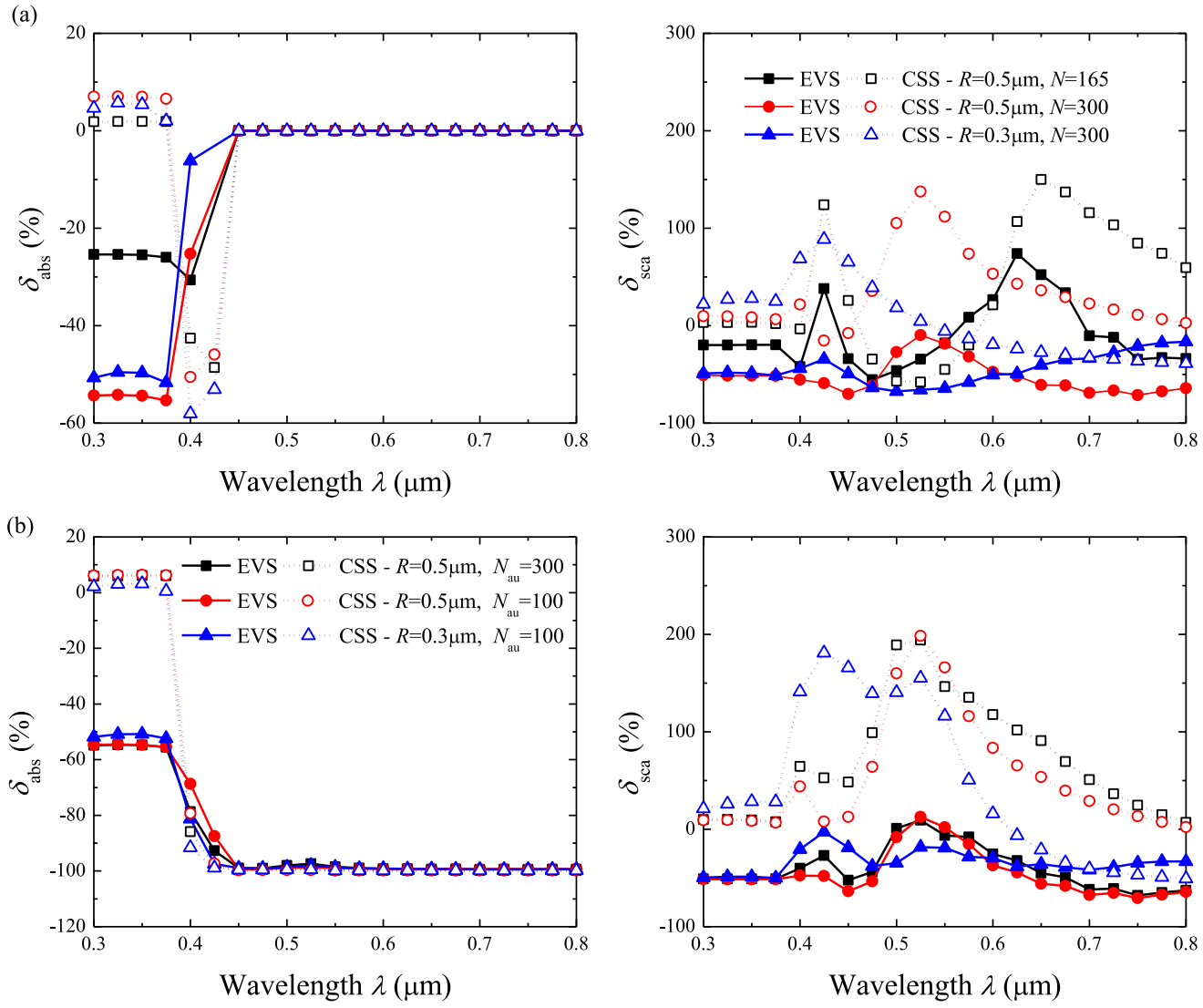

Fig. 12. The relative errors δ of the EVS and the CSS models in estimating the absorption and scattering cross sections of the (a) HPs and (b) HP-Au. The number N of ZnO nanorods is 300 in (b).

where V_i is the volume of the ith component; the subscripts 1, 2 and 3 represent the polystyrene, ZnO and Au, respectively. The corresponding effective dielectric constant ε_{eff} of the EVS model is obtained by the Maxwell-Garnett mixing rule [38,42]:

$$\frac{\varepsilon_{eff}-\varepsilon_1}{\varepsilon_{eff}+2\varepsilon_1}=f_2\frac{\varepsilon_2-\varepsilon_1}{\varepsilon_2+2\varepsilon_1}+f_3\frac{\varepsilon_3-\varepsilon_1}{\varepsilon_3+2\varepsilon_1} \quad (2)$$

where f_i and ε_i are the volume fraction and dielectric constant of the ith component.

As to the CSS model, the inner core is the polystyrene sphere with radius R and the outer shell represents the spike zone with radius $R+l$. The outer shell of the CSS model incorporates the surrounding medium in it; the corresponding effective dielectric constant ε_{eff} of the shell is also obtained by the Maxwell-Garnett mixing rule [38,42]:

$$\frac{\varepsilon_{eff}-\varepsilon_0}{\varepsilon_{eff}+2\varepsilon_0}=f_2\frac{\varepsilon_2-\varepsilon_0}{\varepsilon_2+2\varepsilon_0}+f_3\frac{\varepsilon_3-\varepsilon_0}{\varepsilon_3+2\varepsilon_0} \quad (3)$$

where ε_0 is the surrounding medium.

Meanwhile, the relative error δ of the integral radiative parameters approximated by the EVS and CSS models is defined as:

$$\delta_\chi=\frac{\chi_S-\chi}{\chi}\times 100\% \quad (4)$$

where χ refers to C_{abs}, C_{sca}, ω and g of HPs or HP-Au calculated by the DDA method; χ_S refers to C_{abs}, C_{sca}, ω and g of the EVS and the CSS model calculated by the Mie theory [21].

Fig. 12(a) illustrates the relative errors of the EVS and CSS models in estimating the absorption and scattering cross sections of the HPs. In the spectral range from 0.3 to 0.375 μm, as shown in Fig. 12(a), the CSS model overestimates the absorption cross section of HPs with relative errors less than 10%, whereas the EVS model underestimate the absorption cross section with relative errors larger than 50% for HPs with 300 ZnO nanorods. In the spectral range from 0.375 to 0.45 μm, the relative errors of the absorption cross section of the EVS model are smaller than those of the CSS model. The relative errors of both the CSS and EVS models were zero in the spectral range from 0.45 to 0.8 μm, since polystyrene and ZnO have no absorption in this spectral range. As to the scattering cross section, the relative errors of the CSS model are less than 25% in the spectral range from 0.3 to 0.375 μm, while in the visible spectral range it can be almost 150% since the CSS model fails to predict the sharp peak of the scattering cross section of HPs. In addition, it seems that EVS performs better than CSS in predicting the absorption cross section with relative errors smaller than 60%. Fig. 12(b) shows the relative errors of absorption

and scattering cross section of HP-Au approximated by the EVS and CSS models with different geometrical parameters. As shown in Fig. 12(b), the performances of the two simplified equivalent spheres for HP-Au are similar to those for HPs. Moreover, the relative errors for the absorption cross section are almost 100% in the visible spectral range, indicating that EVS and CSS cannot reproduce the strong absorption by the Au nanoparticles. Overall, both the EVS and the CSS models fail to reproduce the absorption and scattering cross sections of HPs and HP-Au.

5. Conclusion

In this work, we have built models of HP-Au and calculated the radiative properties of HP-Au in the spectral range from 0.3 to 0.8 μm using DDA. The morphological effect on the radiative properties of HP-Au is studied in detail, as an effort to optimize the HP-Au morphology in terms of light absorption for the application of photocatalysis.

The light absorption of HPs is the precondition for the photocatalysis reaction in the ultraviolet spectral range. HPs with lankier ZnO nanorods exhibit larger light absorption in the spectral range from 0.3 to 0.4 μm. For HPs with up to 300 ZnO nanorods, the absorption cross section is about 5 μm^2, which is five times that of the equivalent volume sphere. The radiative properties of HPs largely depend on the surface spike-like structure. The effect of Au nanoparticles on the radiative properties of HP-Au is significant in the visible spectral range, whereas it is negligible in the spectral range from 0.3 to 0.4 μm. In addition, the deposited Au nanoparticles do not increase the light absorption by ZnO. The light absorption of HP-Au in the visible spectral range is only contributed by the Au nanoparticles.

The localized surface plasmon resonance of Au nanoparticles plays a significant role in determining the photocatalysis activity of HP-Au in the visible spectral range. The peak absorption cross section of Au nanoparticles deposited on the HPs is larger than that of the independent one when the Au to Zn mass concentration ratio is below 9%. The enhancement ratio can exceed 1.5 for HP-Au with an Au to Zn mass concentration ratio of 4%. However, for Au to Zn mass concentration ratio larger than 14%, further deposition of Au nanoparticles does not notably increase the absorption cross section of HP-Au which maintains at a value of about 5 μm^2 at the resonance wavelength. With the same amount of deposited Au nanoparticles, HP-Au with larger particle size have larger absorption cross section. In addition, both the EVS and CSS model fail to reproduce the absorption and scattering cross sections of HPs and HP-Au in the visible spectral range, the relative errors of which can be larger than 100%.

Acknowledgments

We acknowledge the support by National Natural Science Foundation of China (Nos. 51336002, 51421063).

References

[1] Mahian O, Kianifar A, Kalogirou SA, Pop I, Wongwises S. A review of the applications of nanofluids in solar energy. Int J Heat Mass Transfer 2013;57:582–94.
[2] Gorji TB, Ranjbar AA. A review on optical properties and application of nanofluids in direct absorption solar collectors (DASCs). Renew Sust Energ Rev 2017;72:10–32.
[3] An W, Wu J, Zhu T, Zhu Q. Experimental investigation of a concentrating PV/T collector with Cu_9S_5 nanofluid spectral splitting filter. Appl Energy 2016;184:197–206.
[4] An W, Li J, Ni J, Taylor RA, Zhu T. Analysis of a temperature dependent optical window for nanofluid-based spectral splitting in PV/T power generation applications. Energy Convers Manage 2017;151:23–31.
[5] Keller AA, Wang H, Zhou D, Lenihan HS, Cherr G, Cardinale BJ, et al. Stability and aggregation of metal oxide nanoparticles in natural aqueous matrices. Environ Sci Technol 2010;44:1962.
[6] Okada Y, Kokhanovsky AA. Light scattering and absorption by densely packed groups of spherical particles. J Quant Spectros Radiat Transfer 2009;110:902–17.
[7] Jassby D, Farner BJ, Wiesner M. Impact of aggregate size and structure on the photocatalytic properties of TiO_2 and ZnO nanoparticles. Environ Sci Technol 2012;46:6934–41.
[8] Bahng JH, Yeom B, Wang Y, Tung SO, Hoff JD, Kotov N. Anomalous dispersions of 'hedgehog' particles. Nature 2015;517:596–9.
[9] Xuan Y, Duan H, Li Q. Enhancement of solar energy absorption using a plasmonic nanofluid based on TiO_2/Ag composite nanoparticles. RSC Adv 2014;4:16206–13.
[10] Cushing SK, Li J, Meng F, Senty TR, Suri S, Zhi M, et al. Photocatalytic activity enhanced by plasmonic resonant energy transfer from metal to semiconductor. J Am Chem Soc 2012;134:15033–41.
[11] Linic S, Christopher P, Ingram DB. Plasmonic-metal nanostructures for efficient conversion of solar to chemical energy. Nat Mater 2011;10:911–21.
[12] Hartland GV, Besteiro LV, Johns P, Govorov AO. What's so hot about electrons in metal nanoparticles? ACS Energy Lett 2017;2:1641–53.
[13] Georgekutty R, Seery MK, Pillai SC. A Highly efficient Ag-ZnO photocatalyst: synthesis, properties, and mechanism. J Phys Chem C 2008;112:13563–13570.
[14] Wang X, He Y, Chen M, Hu Y. ZnO-Au composite hierarchical particles dispersed oil-based nanofluids for direct absorption solar collectors. Sol Energy Mater Sol Cells 2018;179:185–93.
[15] Wang X, He Y, Liu X, Zhu J. Synthesis of hierarchical flower-like particles and its application as super-hydrophobic coating. Powder Technol 2017;319:408–14.
[16] Clavero C. Plasmon-induced hot-electron generation at nanoparticle/metal-oxide interfaces for photovoltaic and photocatalytic devices. Nat Photonics 2014;8:95–103.
[17] Sousacastillo A, Comesañahermo M, Rodríguezgonzález B, Pérezlorenzo M, Wang Z, Kong XT, et al. Boosting hot electron-driven photocatalysis through anisotropic plasmonic nanoparticles with hot spots in Au–TiO_2 nanoarchitectures. J Phys Chem C 2016;120:11690–9.
[18] Primo A, Corma A, García H. Titania supported gold nanoparticles as photocatalyst. Phys Chem Chem Phys 2011;13:886–910.
[19] Ingram DB, Christopher P, Bauer JL, Linic S. Predictive model for the design of plasmonic metal/semiconductor composite photocatalysts. ACS Catal 2011;1:1441–7.
[20] Mishchenko MI, Travis LD, Lacis AA. Scattering, absorption, and emission of light by small particles. Cambridge: Cambridge University Press; 2002.
[21] Bohren CF, Huffman DR. Absorption and scattering of light by small particles. New York: John Wiley & Sons; 1983.
[22] Liu X, Xuan Y. Full-spectrum volumetric solar thermal conversion via photonic nanofluids. Nanoscale 2017;9:14854–60.
[23] Lee BJ, Park K, Walsh T, Xu L. Radiative heat transfer analysis in plasmonic nanofluids for direct solar thermal absorption. J Sol Energy Eng 2012;134:021009.
[24] Liu C, Yin Y. Inherent optical properties of pollen particles: a case study for the morning glory pollen. Opt Express 2016;24 A104-A13.
[25] Dong J, Zhao JM, Liu LH. Effect of spine-like surface structures on the radiative properties of microorganism. J Quant Spectros Radiat Transfer 2016;173:49–64.
[26] Mackowski DW, Mishchenko MI. A multiple sphere T-matrix Fortran code for use on parallel computer clusters. J Quant Spectros Radiat Transfer 2011;112:2182–92.
[27] Mackowski DW. A general superposition solution for electromagnetic scattering by multiple spherical domains of optically active media. J Quant Spectros Radiat Transfer 2014;133:264–70.
[28] Yurkin MA, Hoekstra AG. The discrete dipole approximation: an overview and recent developments. J Quant Spectros Radiat Transfer 2007;106:558–89.
[29] Draine BT, Flatau PJ. Discrete-dipole approximation for scattering calculations. J Opt Soc Am A 1994;11:1491–9.
[30] Sullivan DM. Electromagnetic simulation using the FDTD method. New York: John Wiley & Sons; 2013.
[31] Yang P, Liou KN. Finite-difference time domain method for light scattering by small ice crystals in three-dimensional space. J Opt Soc Am A 1996;13:2072–85.
[32] Liu QH. The PSTD algorithm: a time-domain method requiring only two cells per wavelength. Microw Opt Technol Lett 1997;15:158–65.
[33] Liu C, Panetta RL, Yang P. Application of the pseudo-spectral time domain method to compute particle single-scattering properties for size parameters up to 200. J Quant Spectros Radiat Transfer 2012;113:1728–40.
[34] Yurkin MA, Hoekstra AG. The discrete-dipole-approximation code ADDA: capabilities and known limitations. J Quant Spectros Radiat Transfer 2011;112:2234–47.
[35] Ma X, Lu JQ, Brock RS, Jacobs KM, Yang P, Hu XH. Determination of complex refractive index of polystyrene microspheres from 370 to 1610 nm. Phys Med Biol 2003;48:4165–72.
[36] Adachi S. The handbook on optical constants of semiconductors. Singapore: World Scientific; 2012.
[37] Palik ED. Handbook of optical constants of solids. New York: Academic Press; 1985.
[38] Mishchenko MI, Hovenier JW, Travis LD. Light scattering by nonspherical particles: theory, measurements, and applications. New York: Academic Press; 2000.

[39] Yurkin MA, Kanter DD, Hoekstra AG. Accuracy of the discrete dipole approximation for simulation of optical properties of gold nanoparticles. J Nanophotonics 2010;4:041585.
[40] Wu JJ, Tseng CH. Photocatalytic properties of nc-Au/ZnO nanorod composites. Appl Catal B 2006;66:51–7.
[41] Subramanian V, Wolf EE, Kamat PV. Catalysis with TiO_2/gold nanocomposites. Effect of metal particle size on the Fermi level equilibration. J Am Chem Soc 2004;126:4943–50.
[42] Garnett JCM. Colours in metal glasses, in metallic films, and in metallic solutions. II. Philos Trans R Soc London 1906;205:237–88.